Nanoparticle Direct Doping: Novel Method for Manufacturing Three-Dimensional Bulk Plasmonic Nanocomposites

Marcin Gajc, Hancza B. Surma, Andrzej Klos, Katarzyna Sadecka, Krzysztof Orlinski, Andrey E. Nikolaenko, Krzysztof Zdunek, and Dorota A. Pawlak**

Metallodielectric materials with plasmonic resonances at optical and infrared wavelengths are attracting increasing interest, due to their potential novel applications in the fields of photonics, plasmonics and photovoltaics. However, simple and fast fabrication methods for three-dimensional bulk plasmonic nanocomposites that offer control over the size, shape and chemical composition of the plasmonic elements have been missing. Here, such a manufacturing method and examples of experimental realizations of volumetric isotropic nanocomposites doped with plasmonic nanoparticles that exhibit resonances at visible and infrared wavelengths are presented. This method is based on doping a low-melting dielectric material with plasmonic nanoparticles, using a directional glass-solidification process. Transmission-spectroscopy experiments confirm a homogenous distribution of the nanoparticles, isotropy of the material and resonant behavior. The phenomenon of localized surface plasmon resonance is also observed visually. This approach may enable rapid and cost-efficient manufacturing of bulk nanoplasmonic composites with single or multiple resonances at various wavelength ranges. These composites could be isotropic or anisotropic, and potentially co-doped with other chemical agents, in order to enhance different optical processes.

1. Introduction

Today, materials with negative dielectric permittivity at frequencies below their plasma frequencies are explored for the design and fabrication of novel hybrid materials. These materials have a significant impact on a number of photonic applications. In particular, these materials have led to important developments in the fields of metamaterials[1–3] and nanoplasmonics.[4–6] Examples of unusual electromagnetic properties that have been demonstrated include artificial magnetism,[7,8] the realization of a negative refractive index,[7,9,10] cloaking[11–13] and the squeezing of photons through subwavelength holes.[4] In nanoplasmonics, collective electron oscillations—known as plasmons—at the metal–dielectric interface[4,5] of nanoelements interact with photons at a characteristic frequency and give rise to localized surface plasmon resonances (LSPR). These resonances in turn lead to increased absorption and scattering of light. These effects, together with the local-field enhancement (LFE) around the nanoplasmonic elements, can amplify subsequent optical processes such as photoluminescence, optical nonlinearity and surface-enhanced Raman scattering. The use of plasmons in solar cells,[14] cancer treatment,[15] sensing[16] and plasmon-based lasers[17,18] has already been demonstrated; other applications under investigation include optical information storage,[19] new types of photonic devices,[20] highly efficient light sources[21] and plasmonic metamaterials.[22] The availability of versatile nanoplasmonic materials is therefore of potentially great scientific and economic importance.

Depending on the application, one or more different aspects of the LSPR are critical: the type of enhanced optical property (absorption or scattering); the resonance wavelength distribution (LSPR in the visible and/or infrared range; single, multiple, broadband or tuneable); the enhancement of subsequent optical processes (photoluminescence, up-conversion, nonlinear effects); the geometry of the plasmonic particles (isotropic, anisotropic, single particles, agglomerates); or the macroscopic geometry of the material (layers, volumetric material). The LSPR properties strongly depend on a number of factors, among them the type of nanostructure used, the chemical

M. Gajc, H. B. Surma, Dr. A. Klos, K. Sadecka, K. Orlinski, Prof. D. A. Pawlak
Institute of Electronic Materials Technology
ul. Wolczynska 133, 01-919 Warsaw, Poland
E-mail: Marcin.Gajc@itme.edu.pl; Dorota.Pawlak@itme.edu.pl
Dr. A. E. Nikolaenko
Optoelectronics Research Centre and Centre for Photonic Metamaterials
University of Southampton
Highfield, Southampton, SO17 1BJ, UK
Prof. K. Zdunek
Faculty of Materials Science and Engineering
Warsaw University of Technology
ul. Woloska 141, 02-507 Warsaw, Poland

DOI: 10.1002/adfm.201203116

composition of the nanoplasmonic elements, the environments surrounding the nanoelements, and the size, size distribution, and shape of the nanoelements.[23]

Despite major developments, the fabrication of nanosized metallodielectric structures remains a challenge. Most current fabrication techniques arrange metal nanoparticles on dielectric surfaces. The methods used are either time-consuming and costly (e.g., lithography), or restricted to the creation of two-dimensional structures at a limited production scale. Theoretical proposals[24] for and experimental demonstrations of bottom-up approaches are scarce and (despite demonstrated possibilities of millimetre-scale samples of well-ordered tightly arranged nanoparticles by colloidal chemistry,[25] metal-particle assemblies arranged into liquid crystalline phases,[26] or excitation of leaky waveguided modes in composites processed by electric-field assisted poling,[27] magnetic and Fano-resonances observed in self-assembled nanoparticles clusters,[28–30] and ultrafast optical nonlinearities in gold nanorods assembled via anodized alumina templates),[31] they exhibit significant drawbacks. For example, the optical response in colloidal metallic crystals is broadband and operates in reflection mode, the arrangement of only few-nanometre metal nanoparticles has been demonstrated in liquid crystalline phases, while metallic nanoparticles clusters have been demonstrated only in solutions or as single clusters.

A further approach is based on introducing metal nanoparticles into dielectric materials, typically glasses, to yield three-dimensional bulk materials. There is a number of different methods (i.e., ion exchange, ion implantation, sol-gel, melt quenching, etc.) which are in principle based on doping glasses with metallic ions and in post-processing reducing these ions to metallic nanoparticles (as in the famous example of the Lycurgus cup).[32] We call such methods indirect (chemical) since they incorporate metallic ions into glasses, **Figure 1**, instead of using

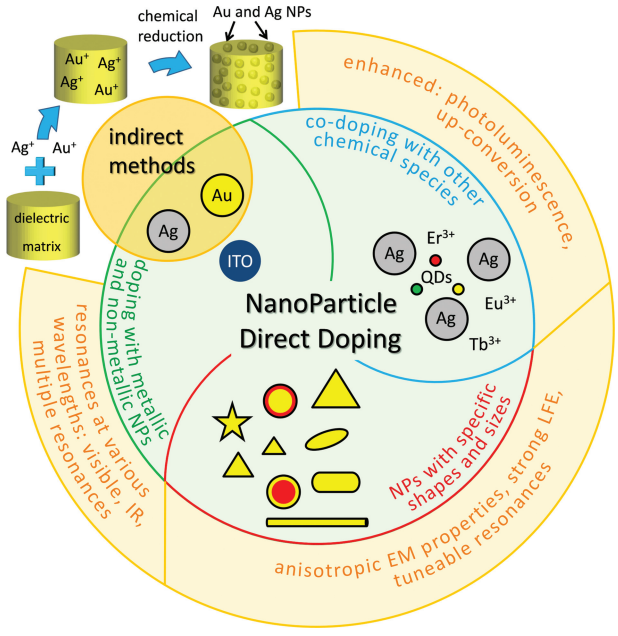

Figure 1. Comparison of the possibilities offered by indirect methods of manufacturing dielectric matrices doped with nanoparticles with nanoparticle direct doping method (NPDD).

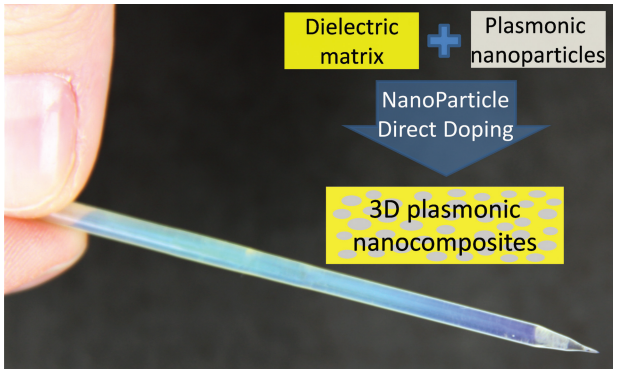

Figure 2. Bulk nanoplasmonic NBP glass rod doped with Ag nanoparticles (NBP:nAg) obtained by nanoparticle direct doping. The diagram depicts the general concept of the manufacturing method.

nanoparticles directly. Indirect methods preclude obtaining materials with nanoparticles of specific sizes and shapes, which is often required for many plasmonic applications. Also these methods can not yield materials with non-metallic particles such as semiconducting particles with smaller (than metallic) losses in the infrared range. Co-doping plasmonic nanoparticles with other chemical species is also not easy to obtain. These constraints can strongly limit further application of the above mentioned methods and manufactured by them materials.

Here we demonstrate a fast, low-cost, bottom-up method for manufacturing nanoplasmonic composites nanoparticle direct doping (NPDD), Figure 1 and **Figure 2**. This method is based on the direct doping of dielectric matrices with plasmonic nanoparticles and enables the fabrication of volumetric three-dimensional materials through a non-chemical process/direct (see Figure 2). The concept is based on utilizing matrices with lower melting temperatures than those of the admixed nanoparticles. In this way, a variety of nanoparticles—of several different sizes, shapes and chemical compositions—can be introduced into the matrix, even when other doping agents such as rare-earth ions are present; see Figure 1. To demonstrate the potential of our method, we present nanoplasmonic composite materials with resonances in the visible and infrared wavelength ranges. Moreover, we report enhanced Er^{3+} photoluminescence in a material co-doped with silver nanoparticles and erbium ions.

2. Results and Discussion

2.1. Fabrication Process

All materials reported here are based on sodium borophosphate dielectric glass ($Na_5B_2P_3O_{13}$, NBP), which serves as the medium. Glass has several advantages over other dielectric materials as a matrix for nanoparticles, including high transparency in the UV–vis range, good mechanical strength, ease of fabrication into desired shapes and sizes, and an amorphous isotropic structure that provides suitable doping conditions. NBP has been chosen as a matrix for the nanoparticles due to its low melting point and wide transparency range.[33]

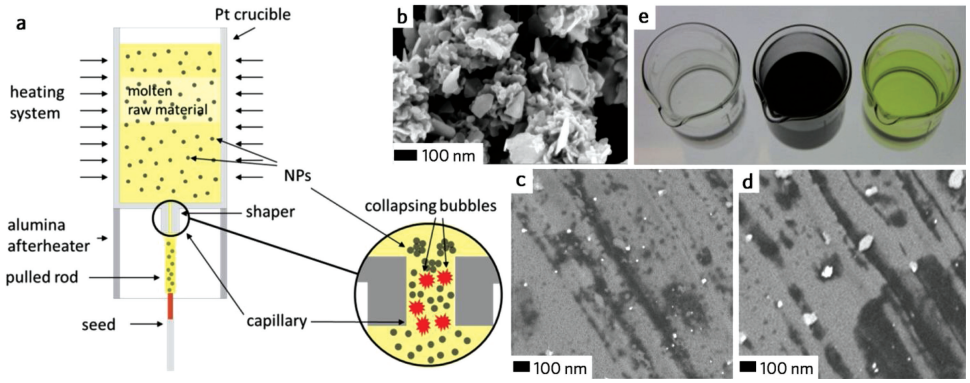

Figure 3. De-agglomeration of Ag nanoparticles during directional solidification using the micro-pulling-down method. a) Scheme of the micro-pulling-down method and of the de-agglomeration process occurring during the nanoparticle direct doping due to the fast flow of the liquid through a capillary, which causes the formation and collapse of bubbles. b) SEM image of the agglomerated Ag nanopowder used for doping the NBP matrix (nominally, spherical particles, 20 nm in diameter). c,d) SEM images of small (c) and large (d) nanoparticles embedded in the NBP matrix after the solidification process using the μ-PD method. e) Comparison of coloration of three solutions (left to right): (i) pure NBP glass dissolved in HCl (aq); (ii) Ag nanopowder mixed in an ultrasonic mixer in isopropanol; the black color is due to Ag agglomerates; (iii) NBP:nAg glass dissolved in HCl (aq), the yellow coloration is due to dispersed Ag nanoparticles.

As plasmonic nanoparticles with resonances in the visible region, we have used commercially available silver nanoparticles (see the Supporting Information). Silver is characterized by one of the highest electrical conductivities and relatively low ohmic losses in the visible-wavelength range, which makes it an attractive plasmonic material. Differential-scanning-calorimetry (DSC) measurements confirmed that Ag nanopowder melts at the same temperature as bulk silver (961.8 °C), and that NBP glass melts at the much lower temperature of 750 °C (see Supporting Information Figure S1), approximately as previously reported (747 °C[33]). Mixing Ag nanopowder with NBP glass in a planetary mill does not significantly influence the melting point of silver. The silver nanopowder we used contained the silver crystallites of 20 nm in average diameter as shown by powder X-ray diffraction and the Scherrer equation. However, scanning-electron-microscopy (SEM) images revealed a strongly agglomerated character of the nanoparticles (**Figure 3**b).

For samples fabrication with NPDD we introduce slightly modified micro-pulling-down (μ-PD) method.[34,35] This method is based on the directional solidification of a melt flowing through a capillary placed in a die at the crucible bottom (Figure 3a). The solidification begins outside of the crucible die after contacting the melt at the die bottom with a seed material due to a substantial but controllable temperature gradient. This method has been previously proposed as a potential method for manufacturing metamaterials.[36–38] Preliminary attempts have also been made to use this method for doping single crystalline matrices with metallic nanoparticles.[39]

For NPDD with micro-pulling down method we used powder of dry nanoparticles. In such form nanoparticles tend to agglomerate as their surface-to-volume ratio is high, leading to strong attractive electrostatic and adhesion forces. A distinct advantage of the μ-PD method is that it helps de-agglomerate the nanoparticles, as they are transported through the nozzle at the center of the crucible die. During the flow of liquid through the capillary, bubble formation (cavitation) and collapsing of formed bubbles (implosion)[40] can occur (Figure 3a). Previous investigations of liquid flows through capillaries have suggested that this phenomenon can lead to separation of nanoparticles originally present as larger agglomerates, as the shock waves are created at the locations of the collapsed bubbles.[41] Following the principle of mass conservation, we calculated the increase of the liquid flow in the capillaries used in our experiments to be at least 50-fold, compared with the flow out of the capillary. This result implies a decrease in pressure inside the capillary, which can lead to the formation of bubbles and their subsequent implosion due to, for example, a sudden increase in pressure at the capillary outlet. An additional process that might help de-agglomeration is the high hydrodynamic shear stress present in the capillaries.[40,41] As a result, the Ag nanoparticles present in the solidified glass rods are not agglomerated (Figure 3d,e). To verify this, we dissolved, our NBP glass doped with Ag nanoparticles in HCl (aq) and found that it exhibited a yellow color, characteristic of dispersed Ag nanoparticles (Figure 3c), in contrast to the black color of agglomerated Ag nanoparticles mixed with isopropanol and the almost colorless solution of undoped NBP glass dissolved in HCl (aq).

2.2. Optical Bulk Plasmonic Nanocomposites

The NBP:nAg rod we have produced exhibits both the LSPR phenomenon in the visible range and a dichroic effect (that is, the phenomenon of different colors in transmission and in scattering; see Supporting Information Video 1). **Figure 4**a depicts transparent and colorless NBP glass rod obtained using the NPDD. After doping the rod with Ag nanoparticles (NBP:nAg), it becomes colored. Figures 4b,c show the NBP-glass rod doped nominally with 0.15 wt.% silver nanoparticles. Against a white background, the observer sees the rod as yellow in the transmitted light. When the rod is placed on a black background, however, light goes through the rod and is absorbed by the background—only scattered light reaches the observer. The material now appears blue. The observed colors originate from the LSPR

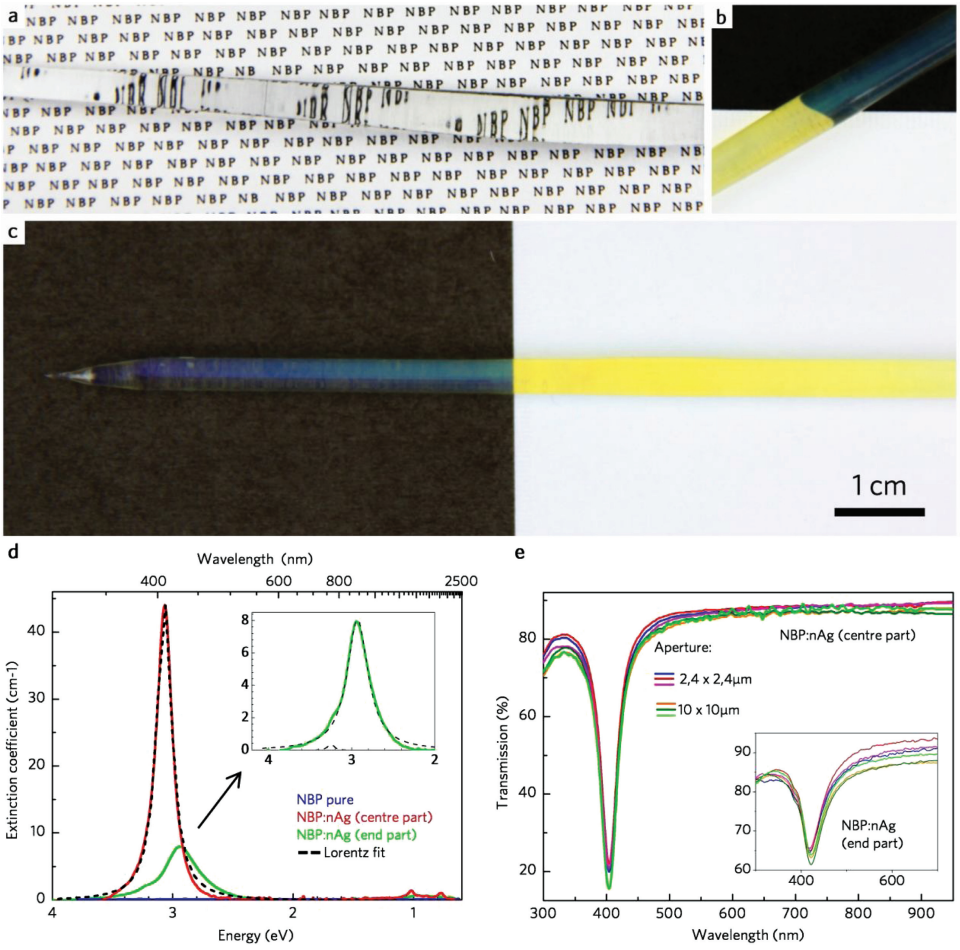

Figure 4. Localized surface plasmon resonance at optical wavelengths in nanoplasmonic NBP:nAg rods obtained using NPDD. a) Pure NBP glass, colorless and transparent. b,c) NBP glass rod doped with 0.15 wt.% of silver nanoparticles, showing yellow coloration on a white background (transmitted light) and blue coloration on a black background (scattered light) due to the LSPR dichroic effect. d) Extinction coefficients of pure NBP and NBP:nAg at two positions along the plasmonic rod, demonstrating the LSPR effect in the visible range; red curve: sample from the centre part of the rod, extinction coefficient max. = 3.07 eV (404 nm), FWHM = 0.15 eV, integrated extinction = 10.6 (eV cm^{-1}); green curve: sample cut from the end of the NBP:nAg rod, extinction coefficient max. = 2.93 eV (423 nm), FWHM = 0.31 eV, integrated extinction = 4 (eV cm^{-1}). e) Demonstration of isotropy and homogeneity of the material via transmission spectra taken in different regions of two samples and with different apertures, showing resonance peaks at the same wavelength. A lens effect is also observed, due to the shape of the glass rod, both in pure NBP (a) and in NBP:nAg color (b).

of the silver nanoparticles, which occurs at a violet-blue wavelength. The absence of perceived green and red components in transmission results from the inability of the human eye to perceive those colors simultaneously, at least under normal conditions.[42] Following the results of Evanoff and Chumanov,[43] we expect that this dichroic effect has two possible origins: the presence of medium-sized nanoparticles in which absorption and scattering occur with similar intensities and in a narrow absorption band, or the presence of a mixture of nanoparticles sizes (for example, 20 nm and >100 nm, respectively) in which the small particles have a strong and sharp absorption peak but the large particles are responsible for broader scattering.

The NBP:nAg rod exhibits a resonance at visible wavelengths, which is manifested as a sharp extinction peak with a maximum at 404 nm (Figure 4d, red curve). The Lorentzian shape of this peak indicates a homogenous broadening of the band, which is of high importance for many applications. The LSPR quality factor, defined[44] as the ratio between the LSPR energy and the LSPR full-width-at-half-maximum (FWHM), is 20.5. Narrower plasmon resonances, thus larger quality factors result from smaller damping. This is important for applications where large field enhancement is necessary, such as photoluminescence.[45] For a sample cut from the conical part at the very end part of the rod, the LSPR wavelength is slightly shifted towards higher values (λ_{max} = 424 nm; green curve in Figure 4d), suggesting the presence of predominately larger Ag particles in this region. This result is also partially confirmed by the coloration of the conical part of the rod, which exhibits very little yellow coloration in transmitted light (see Supporting Information Figure S4) but still shows blue/violet coloration in scattered light (the blue color is darker here than in the other parts of the rod). The differences in the integrated extinction coefficients (4 for small peak compared with 10.6 for the large one) also suggest that in the end region of the rod a smaller concentration of nanoparticles

is present. The quality factor of 9.4 is determined from these results for the end part of the rod.

Transmission spectra taken on a microspectrometer at various sample locations and with different apertures and polarization confirmed the locally homogenous and isotropic distribution of the nanoparticles, as well as the isotropy of the resonance. Figure 4e shows transmission spectra for the same two samples for which the extinction coefficients have been determined (Figure 4d). To verify the homogeneity of the material, the samples were cut from the central part of the rod perpendicular to the solidification direction and from the end part of the rod parallel to the solidification direction (see the Supporting Information). The measurements were taken in different regions of both samples, with apertures of 2.4 μm × 2.4 μm and 10 μm × 10 μm. From the similar appearance of all the transmission spectra for each sample we conclude that the nanoparticle arrangement is rather homogenous in these samples, which were a few millimetres in diameter and in length. However, we note that the technology used here provides centimetre-long rods, and the nanoparticle density is lower at the ends of the rods, presumably due to depletion of the nanoparticles in the melt during the solidification process.

2.3. Infrared Bulk Plasmonic Nanocomposites

As a second example (of advantages of NPDD over the indirect methods), we report bulk nanoplasmonic materials displaying the LSPR phenomenon at infrared wavelengths. These samples were manufactured by direct doping the NBP glass with nanoparticles of transparent conductive oxide. Transparent conductive oxides, such as antimony–tin oxide or indium–tin oxide, are active in the near-infrared region and constitute attractive plasmonic materials, owing to the small negative values of the real part of the permittivity and to low losses.[46,47] These features make them promising candidates for example for transformation-optics and superlens applications.[48]

Figure 5a shows a NBP-glass rod doped with 5 wt% commercially available ATO nanoparticles (see the Supporting Information). At the conditions used in our experiments, we did not achieve a fully homogeneous distribution of the ATO nanoparticles in NBP and areas with larger amounts of particles were observed (Figure 5b). Further optimization of technological parameters, such as applied nozzle, pulling rate, additional rotation of melt in the crucible or of the seed material, may result in homogeneity.

The extinction spectra of the obtained rods (NBP:nATO 2, 5 wt%) display ATO-related broad extinction, with the maxima at ~2.9 μm (Figure 5c). Due to NBP phononic resonance at about 3 and 3.7 μm, the extinction coefficient of NBP glass was subtracted from the spectra of NBP:nATO. The extinction coefficient increases with increasing nanoparticle concentration, an effect that is particularly evident in the differential plots (inset of Figure 5c, and Supporting Information Figure S4).

We have estimated the resonant plasma wavelength of the ATO used in our experiments to be ~1.6 μm. We have prepared an ATO bulk sample by isostatically compressing ATO nanoparticles (identical to those used for doping the NBP glass). For the bulk material, reflection starts around 1.6 μm (Figure 5d). A calculation of the LSPR frequency for the ATO nanoparticles yielded ωLSPR(ATO) ≈ 80 THz (λ ≈ 3.7 μm). We worked with the formula for small spherical plasmonic particles in electrostatic approximation[49] and used ε_M(NBP) ≈ 2.25.[50] The calculated wavelength does not coincide with the value observed experimentally, as a result of the approximated

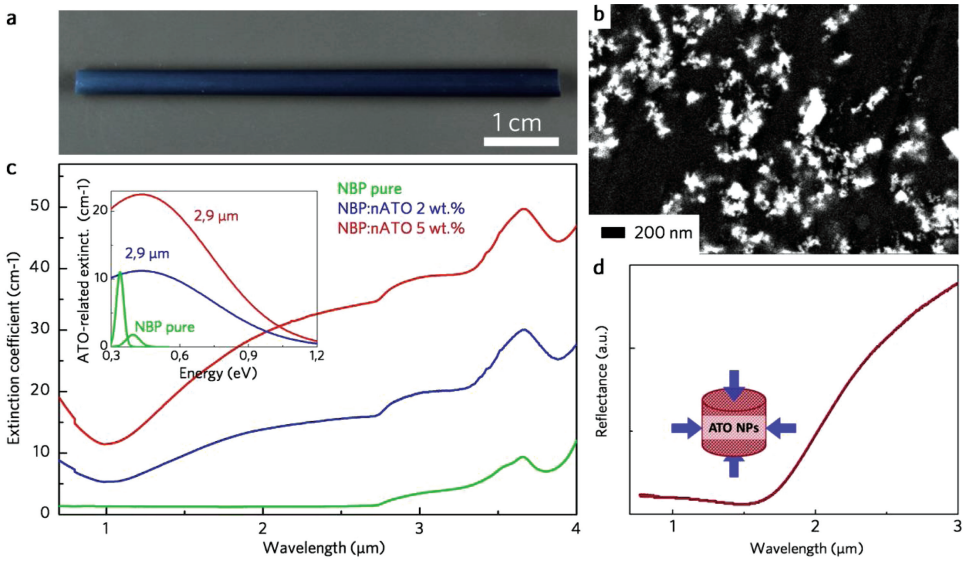

Figure 5. Bulk nanoplasmonic rods with resonances in the IR wavelength range. a) NBP:nATO rod obtained using NPDD. b) SEM image showing an area with densely packed ATO nanoparticles inside the NBP glass. c) Extinction coefficients of pure NBP and NBP:nATO with 2 and 5 wt% of nATO, respectively, indicating increasing extinction with increasing nATO concentration. Inset: ATO-related peaks in comparison with NBP-originated peaks, deconvoluted from the differential-extinction-coefficient (see also Supporting Information Figure S3). d) Reflectance spectra of bulk ATO, composed of isostatically compressed ATO nanoparticles, provide an estimation of the plasma frequency, ω_p(ATO) ≅ 188 THz (1.6 μm).

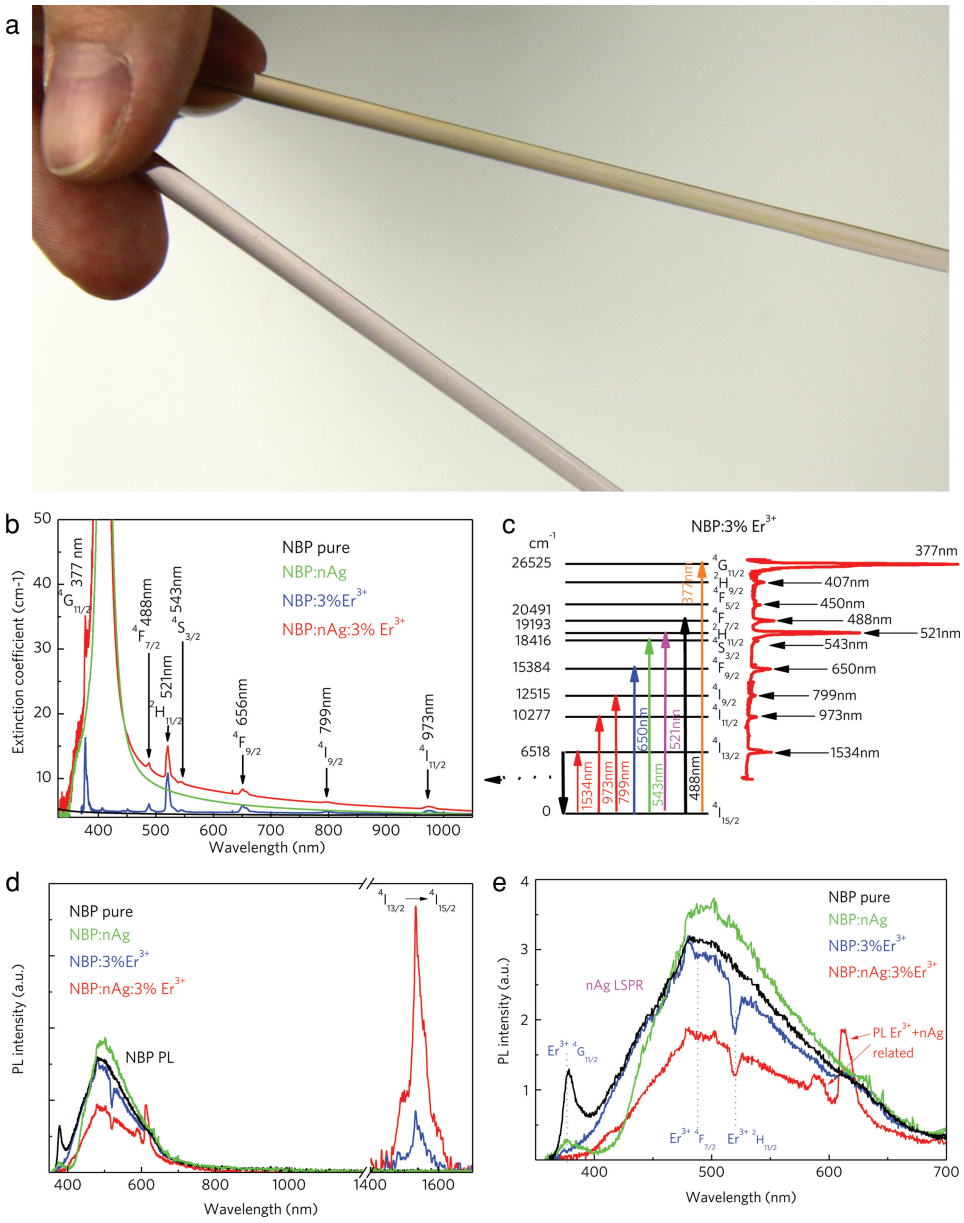

Figure 6. Bulk nanoplasmonic materials co-doped with NBP:nAg,Er^{3+} and their absorption and emission properties. a) NBP:Er^{3+} (pink) and NBP:nAg,Er^{3+} (yellowish-pink) rods obtained using NPsDD. b) Extinction coefficients of pure NBP, NBP:nAg, NBP:Er^{3+} (3 wt.%) and NBP:nAg,Er^{3+} (3 wt%), demonstrating similar Er^{3+} ions absorption in a sample doped only with erbium ions and in a sample co-doped with nAg and Er^{3+} ions. The large peak at ~400 nm originates from the LSPR of the silver nanoparticles; Er^{3+} ions absorption peaks are indicated. c) Energy-level diagram of the Er^{3+} ions with respective Russel–Saunders notation and corresponding absorption spectrum. d) Comparison of photoluminescence properties of pure NBP, NBP:nAg, NBP:Er^{3+} and NBP:nAg,Er^{3+} excited with a 325-nm cw He-Cd laser, demonstrating NBP-originated broadband emission in visible wavelength range for all samples and an increase of 1534 nm PL for the sample co-doped with nAg and Er^{3+} in comparison with the sample doped only with Er^{3+}. The PL intensity for visible wavelengths and IR wavelengths should not be compared. e) A close-up view of the visible PL of NBP:nAg, NBP:Er^{3+} and NBP:nAg,Er^{3}, demonstrating Er^{3+} ions-related absorption and emission peaks in the PL broadband spectrum of NBP. The effect of absorption by nAg due to LSPR is also evident in the PL broadband spectrum of NBP.

character of the applied Drude model,[51] which describes the electromagnetic properties of free carrier materials.

2.4. Co-doped Materials

Next, we explored the possibility of manufacturing materials doped with both nanoparticles and other chemical agents by co-doping NBP rods with Ag nanoparticles and erbium ions, NBP:nAg,Er^{3+} (**Figure 6**a) with NPDD. The extinction spectra of the NBP rod doped with erbium ions alone and the rod doped with both erbium ions and Ag nanoparticles exhibited similar absorption intensities for the erbium lines, indicating similar concentrations of Er^{3+} ions (Figure 6b). In addition, the strong extinction peak due to the LSPR of nAg was observed in both NBP:nAg and NBP:nAg,Er^{3+}.

In NBP:nAg,Er^{3+}, we observed, relative to the NBP:Er^{3+} sample, a seven-fold increase of the 1534-nm Er^{3+} photoluminescence (PL) at room temperature upon excitation with a 325-nm continuous wave He-Cd laser (Figure 6d). Erbium ions do not exhibit a resonant excitation at this pumping wavelength (see Figure 6c). The observed emission from the erbium ions resulted most likely from a strong NBP-matrix emission in the visible spectral range, which was observed in all the samples (Figure 6d). The PL of the matrix causes the absorption of photons by the Er^{3+} ions, whose resonant frequencies (at 488 and 521 nm) overlap with the NBP emission band. Via this indirect route, Er^{3+} PL at 1534 nm may be observed. In addition, the PL band of NBP overlaps with the absorption band of the Ag nanoparticles and causes resonant absorption. Due to a LSPR in the same region as the erbium absorption band (at 377 nm), the overlap between the NBP PL band and the nAg absorption band leads to an increase of the 1534-nm Er^{3+} emission in NBP:nAg,Er^{3+}. The decreased NBP PL at ~400 nm in NBP:nAg (Figure 5e) confirms absorption of the NBP PL by nAg particles. The observed parasitic emission at $\lambda_{max} \approx 613$ nm and 589 nm in these samples suggests the formation of additional radiative recombination centres connected with erbium and nAg.

The bulk samples reported here contain a significantly higher number of active centres than other plasmonic materials reported in the literature. The intensity of PL and rate of up-conversion strongly depends on the concentration of active ions introduced into the matrix. In the materials described here, the calculated erbium concentration is ~2.4×10^{20} ions/cm^3. Previously, concentrations of erbium in plasmonic materials up to 10^{20} ions/cm^3 have been reported.[52] However, taking into account that the materials described in the literature are mainly films, the number of ions available for photoluminescence is much lower, due to the considerably smaller volumes of the films. This leads us to the conclusion that the Er^{3+} PL reported here (without any increase caused by LSPR) is likely to be stronger than that in the previously reported data. Moreover, the average amount of ~2.4 Er^{3+} ions/10 nm^3 suggests a short average distance between the Er^{3+} ions and Ag nanoparticles, thus providing good conditions for photoluminescence enhancement.

3. Discussion and Outlook

Our approach to manufacturing bulk nanoplasmonic composites differs significantly from other techniques for producing nanoparticle-based materials. NPDD offers the possibility of introducing nanoparticles of various chemical compositions into a variety of glasses, and perhaps even other matrices. Particles with plasmonic, polaritonic, and excitonic resonances, as well as nanoparticles with assorted shapes and dimensions, may be used. NPDD also enables the addition of other doping agents, such as rare-earth ions and, potentially, quantum dots. Using this approach, various types of nanoparticles might be combined within the same medium to confer multiple resonances and/or broadband effects. Utilizing nonlinear glasses as a matrix might enhance the nonlinear susceptibilities which in turn might lead to applications such as nonlinear absorbers.

The introduction of rare-earth ions and/or quantum dots should promote the enhancement of important optical properties, including photoluminescence. Glasses doped with rare-earth ions are used in such various applications as lasers, sensors, displays and in the telecommunication industry. However, strong photoluminescence is limited by the quenching effect for higher doping levels and their small absorption cross sections. Enhancement of up-conversion processes could enable new functionalities and/or increased performance of existing devices such as silicon-based solar cells, by introducing, for example, glasses co-doped with nAg and rare-earth ions.[53] Up/down-converters and plasmonics are essential paths in the roadmap of the International Energy Agency toward an increase in photovoltaic energy-conversion efficiency.[54]

An advantage of the materials we describe is that the component particles are protected chemically and mechanically by the matrix. Although the samples presented here come in the form of centimetre-long, millimetre-wide rods, larger sheets could be produced if desired, by working with a crucible with a rectangular die and a slit. Other geometries are also possible. The observed de-agglomeration and self-dispersion of plasmonic nanoparticles suggests the broader possibility of utilising well-established crystal/glass-pulling techniques for manufacturing new materials and thus promises easier transfer of such technologies from the laboratory to industry.

4. Experimental Section

Directional solidification: The bulk nanoplasmonic materials were grown at the Institute of Electronic Materials Technology (ITME) in Warsaw. The raw materials were prepared as follows: (i) A $Na_5B_2P_3O_{13}$ (NBP) glass matrix was prepared from high-purity Na_2CO_3 (99.99%), $NH_4H_2PO_4$ (analytically pure), and H_3BO_3 (99.99%) in a 2.5:3:2 molar ratio. The material was mixed in an alumina mortar and synthesised at 850 °C; (ii) Commercially available Ag nanoparticles (nominally spherical, 20 nm in diameter, and of 99.9% purity by Nanostructurated & Amorphous Materials, Inc. Houston, USA) and ATO nanoparticles (SnO_2:Sb_2O_3, 90:10 wt%, nominally spherical, 40 nm in diameter, 99.5+% purity by SkySpring Nanomaterials, Inc. Houston, USA) were used. (iii) The final raw material was prepared by mixing appropriate amounts of the powdered glass matrix and the respective nanoparticles using an alumina mortar and/or a planetary mill. The original silver nanopowder was agglomerated. After manual mixing, many silver agglomerates were still present. After mixing in the planetary mill, the agglomerates were partially separated, and the particles got pressed into the surface of glass fragments. After introducing the raw materials into the crucible (during the solidification process) and heating it up, convection provided for further mixing of the material. The micro-pulling-down method was used for the solidification process, employing commercial μ-PD growth equipment (Cyberstar). Thanks to the rotational convection forces inside the crucible, the molten material is mixed before the solidification process begins. Inductive heating has been used, and the experiments were carried out both in nitrogen and in air atmospheres. Platinum, iridium and Al_2O_3 (with a heating Ir cylinder) crucibles and alumina afterheaters have been used. The applied pulling rates ranged from 0.5 to 3 mm/min. The μ-PD equipment enables the growth of rods up to 45 cm long. The μ-PD method enables temperature gradients up to 300 °C/mm.[35]

Compositional and Structural Analysis: Powder XRD measurements were performed on the as-grown samples using a Siemens D500 difractometer equipped with a semiconductor Si:Li detector, using KαCu radiation. The powder diffraction pattern was measured using the $\theta/2\theta$ scanning mode with a step size of 0.02° and a counting time

of 10 s/step. The average Ag nanoparticles diameter in the applied Ag nanopowder was calculated using the Scherrer formula.

Thermal Analysis: Calorimetric and thermogravimetric measurements were performed on a STA 449 F1 (NETZSCH) with a platinum furnace and using the following (flowing) gas mixture: argon (20 mL/min) and nitrogen (20 mL/min). The signal was measured using a Pt–Rh thermocouple, and platinum crucibles were used in a temperature range from ambient to 1373 K with a heating rate of 10 K/min. An exception was made for silver, for which alumina crucibles were used. The sample masses varied from 45 mg (NBP and NBP-Ag nanocomposite) to 60 mg (silver nanopowder). Temperatures were extracted from the plots based on their onset (melting and crystallization).

Electromagnetic Characterization: The optical transmission spectra of NBP:nAg samples were measured using a microspectrometer (CRAIC) available at the University of Southampton, UK. To verify the homogeneity of the material, samples were cut from the central part of the rod (round, approximately 3 mm in diameter, thickness 368 μm) perpendicular to the solidification direction and from the end part of the rod (rectangular, 3 mm × 5 mm, thickness 410 μm) parallel to the solidification direction. The distance between samples was approximately 6 cm along the axis of the rod. The size of the sampling area varied from 2.4 μm × 2.4 μm to 42 μm × 42 μm. Other transmission/extinction measurements were performed on Carry500 and Fourier VERTEX 80 spectrophotometers, available in ITME.

Photoluminescence Characterization: The photoluminescence spectra were excited with a 325-nm cw He-Cd laser and recorded using a double grating monochromator HR460 and the lock-in technique, with a resolution 0.7 nm at 600 nm. The PL signal was collected by a cooled photomultipliers, EMI- 9658BM and Hamamatsu 5509–72.

Additional Information: The authors have applied for a patent regarding this work.

Supporting Information

Supporting Information is available from the Wiley Online Library or from the author.

Acknowledgements

The authors thank the FP7 NMP ENSEMBLE Project (GA NMP4-SL-2008-213669), the TEAM Programme operated within the Foundation for Polish Science co-financed by the EU European Regional Development Fund, and MAESTRO Project (2011/02/A/ST5/00471) operated by National Science Centre for support of this work. The authors acknowledge the COST Action MP0803 and the UK's Engineering and Physical Sciences Research Council under the Nanostructured Photonic Metamaterials Programme grant EP/G060363/1 for support. The authors would also like to thank Dr. Iwona Jozwik (ITME) for her help with SEM images, Dr. Ryszard Diduszko (ITME) for his help with XRD measurements, Dr. Ryszard Stepien (ITME) for his advice on glass, Dr. Piotr Nyga (Military University of Technology, Warsaw, Poland) for helpful discussions, Prof. William L. Barnes (University of Exeter, UK) for his great suggestion of preparing a video for a better visualisation of the dichroism of the NBP:Ag rod, Dr. Mark Waller (University of Münster, Germany) for narrating the Supporting Video, and Dr. Sian Howard (Institut Für Sprachen Kassel, Germany) for producing the background music.

Received: October 24, 2012
Revised: December 23, 2012
Published online: February 15, 2013

[1] R. M. Walser, *Proc. SPIE* **2001**, *4467*, 1–15.
[2] D. R. Smith, J. B. Pendry, M. C. K. Wiltshire, *Science* **2004**, *305*, 788–792.
[3] N. I. A. Zheludev, *Opt. Photonics News* **2011**, *22*, 30–35.
[4] W. L. Barnes, A. Dereux, T. W. Ebbesen, *Nature* **2003**, *424*, 824–830.
[5] J. A. Schuller, E. S. Barnard, W. Cai, Y. Ch. Jun, J. S. White, M. Brongersma, *Nat. Mater.* **2010**, *9*, 193–204.
[6] D. K. Gramotnev, S. I. Bozhevolny, *Nat. Photonics* **2010**, *4*, 83–91.
[7] J. B. Pendry, A. J. Holden, D. J. Robbins, W. J. Stewart, *IEEE transactions on microwave theory and techniques* **1999**, *47*, 2075–2084.
[8] S. Linden, Ch. Enkrich, M. Wegener, J. Zhou, T. Koschny, C. M. Soukoulis, *Science* **2004**, *306*, 1351–1353.
[9] V. M. Shalaev, *Nat. Photonics* **2007**, *1*, 41–48.
[10] C. M. Soukoulis, S. Linden, M. Wegener, *Science* **2007**, *315*, 47–49.
[11] D. Schurig, J. J. Mock, B. J. Justice, S. A. Cummer, J. B. Pendry, A. F. Starr, D. R. Smith, *Science* **2006**, *314*, 977–980.
[12] W. Cai, U. K. Chettiar, A. V. Kildishev, V. M. Shalaev, *Nat. Photonics* **2007**, *1*, 224–227.
[13] M. W. McCall, A. Favaro, P. Kinsler, A. Boardman, *J. Opt.* **2011**, *13*, 024003.
[14] H. A. Atwater, A. Polman, *Nat. Mater.* **2010**, *9*, 205–213.
[15] S. Lal, S. E. Clare, N. J. Halas, *Acc. Chem. Res.* **2008**, *41*, 1842–1851.
[16] J. N. Anker, W. P. Hall, O. Lyandres, N. C. Sahah, J. Zhao, R. P. Van Duyne, *Nat. Mater.* **2008**, *7*, 442–453.
[17] M. Stockman, D. J. Bergman, *Phys. Rev. Lett.* **2003**, *90*, 027402.
[18] M. A. Noginov, G. Zhu, A. M. Belgrave, R. Bakker, V. M. Shalaev, E. E. Narimanov, S. Stout, E. Herz, T. Suteewong, U. Wiesner, *Nature* **2009**, *460*, 1110–1112.
[19] D. O'Connor, A. V. Zayats, *Nat. Mater* **2010**, *5*, 482–483.
[20] A. Hryciw, Y. Ch. Jun, M. Brongersma, *Nat. Mater* **2010**, *9*, 3–4.
[21] K. Okamoto, I. Niki, A. Shvartser, Y. Narukawa, T. Mukai, A. Scherer, *Nat. Mater.* **2004**, *3*, 601–605.
[22] J. Henzie, M. H. Lee, T. W. Odom, *Nat. Nanotechnol.* **2007**, *2*, 549–554.
[23] W. A. Murray, W. L. Barnes, *Adv. Mater.* **2007**, *19*, 3771–3782.
[24] C. Rockstuhl, T. Scharf, *J. Microsc.* **2008**, *229*, 281–286.
[25] A. Tao, P. Sinsermsuksakul, P. Yang, *Nat. Nanotechnol.* **2007**, *2*, 435–440.
[26] M. Wojcik, M. Góra, J. Mieczkowski, J. Romiszewski, E. Górecka, D. Pociecha, *Angew. Chem. Int. Ed.* **2009**, *48*, 5167–5169.
[27] M. Beresna, P. G. Kazansky, O. Deparis, I. C. S. Carvalho, S. Takahashi, A. V. Zayats, *Adv. Mater.* **2010**, *22*, 4368–4372.
[28] J. A. Fan, C. Wu, K. Bao, J. Bao, R. Bardhan, N. J. Halas, V. N. Manoharan, P. Nordlander, G. Shvets, F. Capasso, *Science* **2010**, *328*, 1135–1138.
[29] S. Mühlig, A. Cunningham, S. Scheeler, C. Pacholski, T. Bürgi, C. Rockstuhl, F. Lederer, *ACS Nano* **2011**, *5*, 6586–6592.
[30] S. J. Tan, M. J. Campolongo, D. Luo, W. Cheng, *Nat. Nanotechnol.* **2011**, *6*, 268–276.
[31] G. A. Wurtz, R. Pollard, W. Hendren, G. P. Wiederrecht, D. J. Gosztola, V. A. Podolskiy, A. V. Zayats, *Nat. Nanotechnol.* **2011**, *6*, 107–111.
[32] U. Leonhardt, *Nat. Photonics* **2007**, *1*, 207–208.
[33] C. Hauf, A. Yilmaz, M. Kizilyalli, R. Kniep, *J. Solid State Chem.* **1998**, *140*, 154–156.
[34] D. H. Yoon, I. Yonenaga, N. Ohnishi, T. Fukuda, *J. Cryst. Growth* **1994**, *142*, 339–343.
[35] *Shaped crystals: Growth* by the Micro-pulling-down Technique (Ed: T. Fukuda, V. I. Chani), Springer-Verlag, Berlin Heidelberg **2007**.
[36] D. A. Pawlak, K. Kolodziejak, S. Turczynski, J. Kisielewski, K. Rozniatowski, R. Diduszko, M. Kaczkan, M. Malinowski, *Chem. Mater.* **2006**, *18*, 2450–2457.
[37] D. A. Pawlak, Self-organized structures for metamaterials. in *Handbook of Artificial Materials Vol. 2.* (Ed. F. Capolino) Taylor & Francis: Oxford, UK **2009**.
[38] D. A. Pawlak, S. Turczynski, M. Gajc, K. Kolodziejak, R. Diduszko, K. Rozniatowski, J. Smalc, I. Vendik, *Adv. Funct. Mater.* **2010**, *20*, 1116–1124.

[39] A. Klos, M. Gajc, R. Diduszko, D. A. Pawlak, 11th International Conference on Transparent Optical Networks, **2009** *1–2*, 421–424.
[40] J. Li, P. Cheng, *Int. J. Heat Mass Trans.* **2004**, *47*, 2689–2698.
[41] J. Baldyga, Ł. Makowski, W. Orciuch, C. Sauter, H. P. Schuchmann, Proc.13th Eur. Conf. On Mixing, London *14–17*, 04.2009.
[42] H. D. Crane, T. P. Piantanida, *Science* **1983**, *221*, 1078–1080.
[43] D. D. Evanoff Jr., G. Chumanov, *J. Phys. Chem. B* **2004**, *108*, 13957–13962.
[44] J. M. Luther, P. K. Jain, T. Ewers, A. P. Alivisatos, *Nat. Mater.* **2011**, *10*, 361–366.
[45] K. Munechika, J. M. Smith, Y. Chen, D. S. Ginger, *J. Phys. Chem. C* **2007**, *111*, 18906–1891.
[46] M. Kanehara, H. Koike, T. Yoshinaga, T. Teranishi, *J. Am. Chem. Soc.* **2009**, *131*, 17736–17737.
[47] T. Nütz, U. zum Felde, M. Haase, *J. Chem. Phys.* **1999**, *110*, 12142–12150.
[48] P. R. West, S. Ishii, G. V. Naik, N. K. Emani, V. M. Shalaev, A. Boltasseva, *Laser Photonics Rev.* **2010**, *4*, 795–808.
[49] U. Kreibig, M. Vollmer, *Optical Properties of Metals Cluster*, Springer-Verlag, Berlin **1995**.
[50] E. T. Y. Lee, E. R. M. Taylor, *J. Phys. Chem. Solids* **2005**, *66*, 47–51.
[51] B. Drude, *Ann. Phys.* **1900**, *1*, 566–613.
[52] E. Trave, G. Mattei, P. Mazzoldi, G. Pellegrini, C. Scian, C. Maurizio, G. Battaglin, *Appl. Phys. Lett.* **2006**, *89*, 151121.
[53] S. Pillai, M. A. Green, *Sol. Energy Mater. Sol. Cells* **2010**, *94*, 1481–1486.
[54] http://www.iea.org/publications/freepublications/publication/pv_roadmap.pdf